Supporting Information

Unveiling the Advantages of Ultrathin N-Doped Carbon Shell on Self-Supported Tungsten Phosphide Nanowire Arrays for Hydrogen Evolution Reaction Experimentally and Theoretically

Cuncai Lv[a,b], Jifeng Liu[a], Pingping Lou[a], Xiaobo Wang[a], Linjie Gao[a], Shufang Wang[a], Zhipeng Huang[b*]*

[a] Key Laboratory of High-precision Computation and Application of Quantum Field Theory of Hebei Province, Institute of Life Science and Green Development, The College of Physics Science and Technology, Hebei University, Baoding 071002, P. R. China.

[b] School of Chemical Science and Engineering, Institute for Advanced Study, Tongji University, Shanghai, 200092, P. R. China.

* Shufang Wang, E-mail: fwang@hbu.edu.cn; Zhipeng Huang, E-mail: zphuang@tongji.edu.cn.

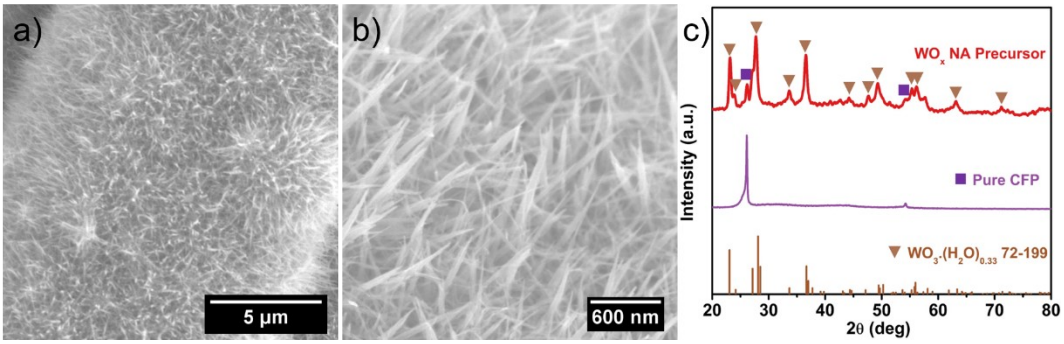

Figure S1. (a) Low- and (b) high-magnification SEM images of WO_x NA precursor loaded on CFP. (c) XRD pattern of WO_x NA precursor on CFP.

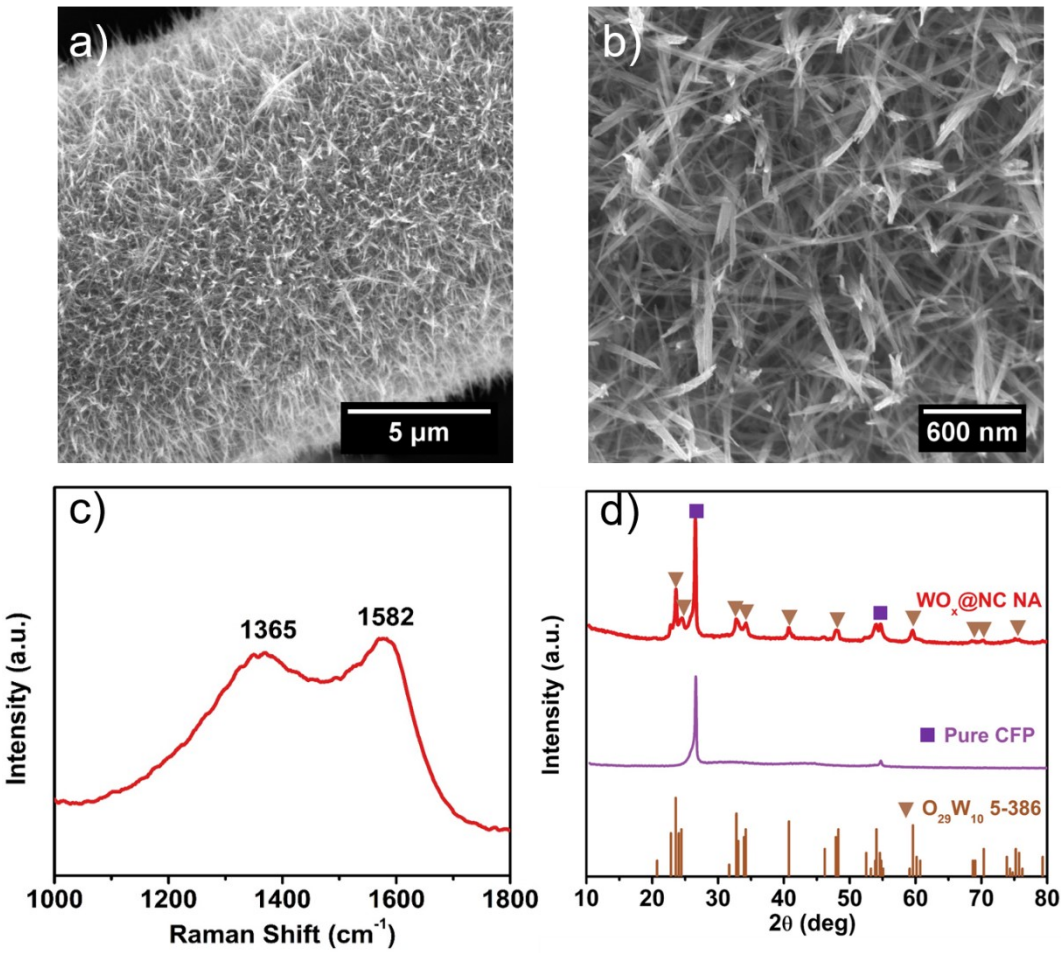

Figure S2. (a) Low- and (b) high-magnification SEM images of WO_x@NC NA loaded on CFP. (c) Raman spectrum of WO_x@NC NA loaded on Ti foil. (d) XRD pattern of WO_x@NC NA loaded on CFP.

Supporting Discussion S1. Estimation of the carbon weight content in WP@NC NA

The WP@NC NA and WP NA were exfoliated from the Ti foil via scarping, and subjected to thermogravimetric analysis (TGA). All WP (x) were oxidized to WO_x (1.2352x), and all carbon layer (1-x) was removed during the oxidation process at 800 °C. The weight percent of WP in WP@NC NA is computed according to the follow equation:

$$1.2352x-(1-x)=1.0541$$

Where x is the weight percent of WP, 1-x is the weight percent of carbon layer. According to the equation, x is computed to be 91.9%. Therefore, the weight percent of carbon layer is 1 – 91.9% = 8.1%.

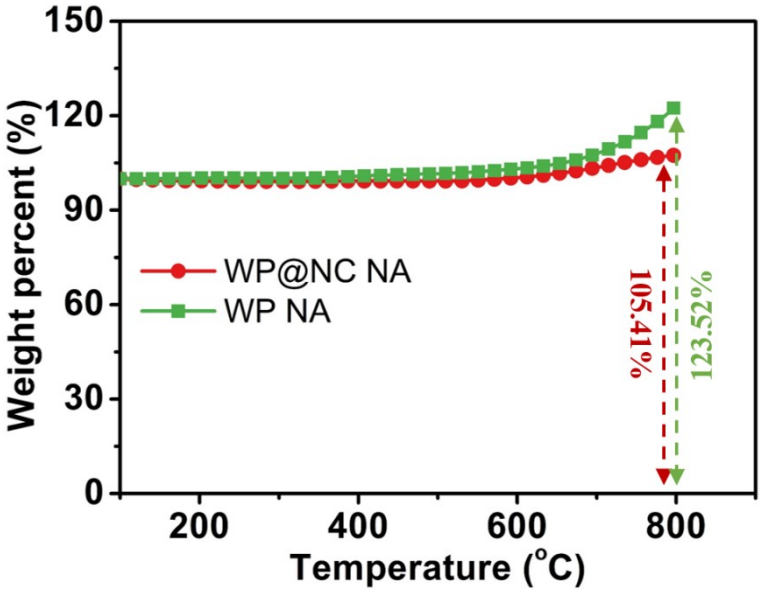

Figure S3. TGA curves of WP@NC NA and WP NA measured in O_2 atmosphere.

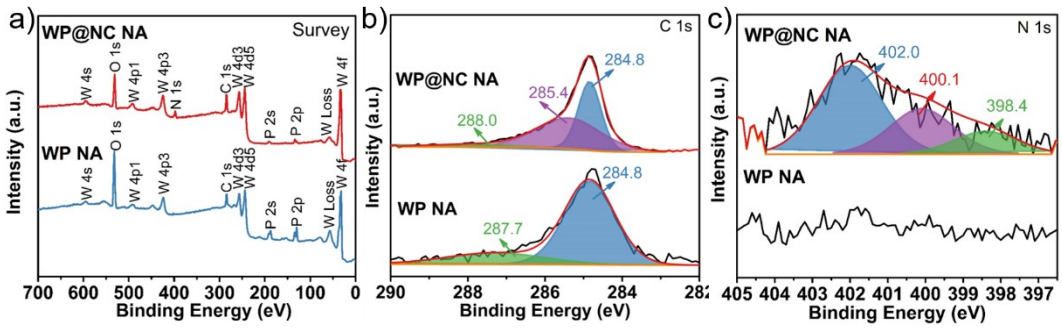

Figure S4. (a) Survey, (b) W 4f window and (c) P 2p window of the XPS spectra of WP@NC NA and WP NA.

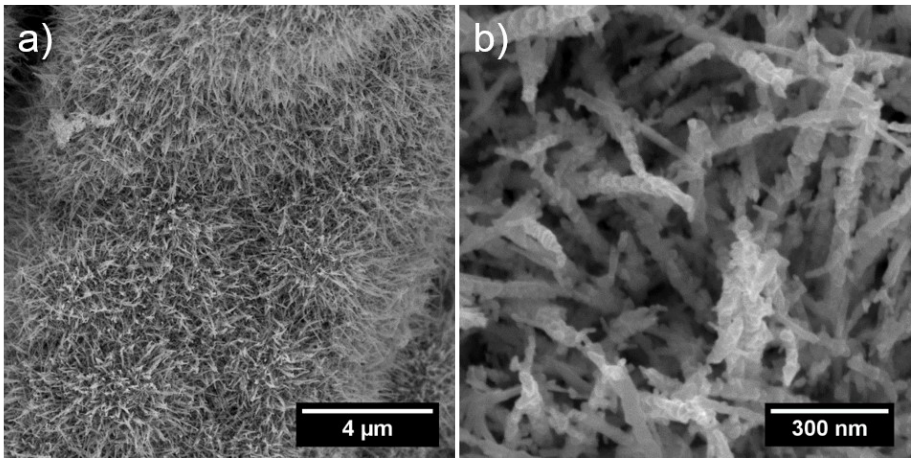

Figure S5. (a) Low- and (b) high-magnification SEM images of WP NA-s.

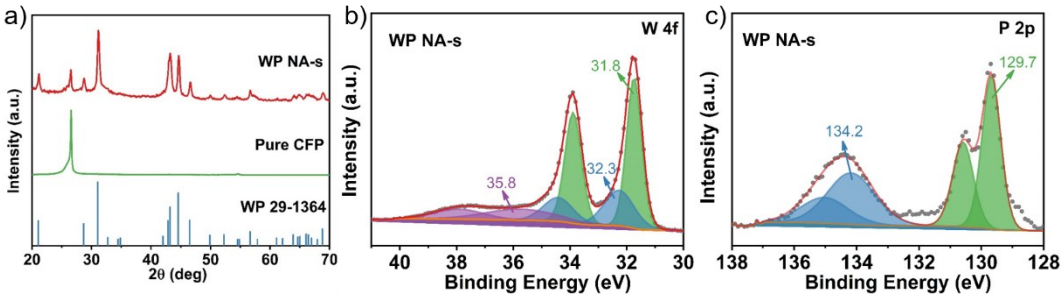

Figure S6. (a) XRD pattern of WP NA-s. (b) W 4f window and (c) P 2p window of the XPS spectra of WP NA-s.

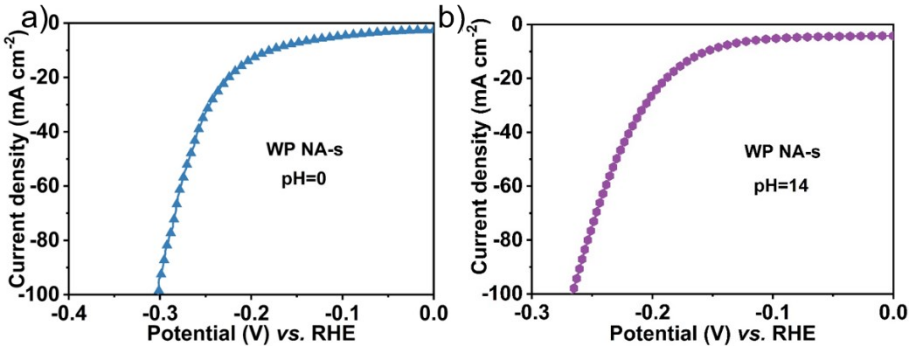

Figure S7. Polarization curves for the WP NA-s in (a) 0.5 M H_2SO_4 and (b) 1 M KOH. All the potentials were corrected by iR drop.

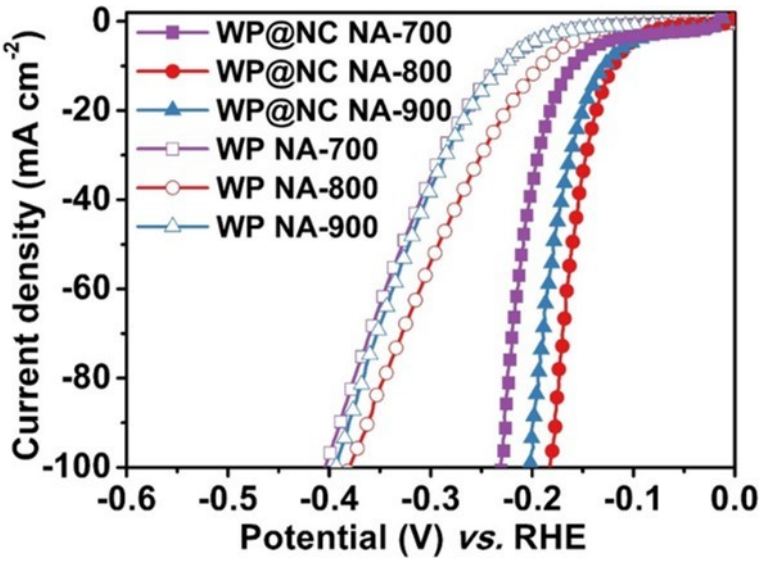

Figure S8. Polarization curves of WP@NC NA and WP NA obtained under different phosphidation temperatures (denoted as WP@NC NA-xx and WP NA-xx, where xx is the phosphidation temperature) in 0.5 M H_2SO_4. In the whole article, WP@NC NA-800 and WP NA-800 are also denoted as WP@NC NA and WP NA, respectively.

Table S1. Comparison of the HER activities of WP@NC NA with some representative highly efficient metal phosphides-based electrocatalysts in 0.5 M H_2SO_4 electrolyte.

Catalyst	Counter electrode	η_{10} (mV)	η_{100} (mV)	Tafel slope (mV/dec)	Stability (h)	Reference
3D MoP/NPG	Pt wire	148	>300	49	60	[1]
MoP@NC	Graphite rod	52	~165	49	10	[2]
WP@NC		173	--	84	--	
Co-WP	Graphite rod	98	--	51	60	[3]
Mo-WP		139	--	65	60	
Termed Cu_3P@NPPC	Pt wire	89	>210	76	11	[4]
Re_2P@NPVC	Carbon rod	55	~200	43	100	[5]
Re_3P_4@NPVC		40	~180	38	100	
N-MoP/CC	Graphite rod	~130	~250	--	--	[6]
CoP@NPC/CP	Pt wire	~110	>300	82	10	[7]
MoP/NC	Carbon rod	183	>250	56.9	12	[8]
WP_2 SMPs	Graphite rod	161	294	57	22	[9]
CoWP-CA/KB	Platinum plate	111	>300	58	60	[10]
Mo-W-P/CB	Graphite rod	165	>250	62	12	[11]
Ce-doped CoP	Graphite rod	54	~120	54	10	[12]
$Co_{0.9}W_{1.1}P_2$/C	Graphite rod	35	--	34	50	[13]
WP	Pt wire	314	>350	95.71	24	[14]
α-WP_2		271	>300	86.83	24	
CFs@WP	Graphite rod	137	215	69	24	[15]
2D ultrathin FeP	Graphite rod	117	>180	56	15	[16]
LC-WP	Carbon rod	170	>200	52	30	[17]
WP_2 NS/CC	Graphite rod	140	250	85	27	[18]
WP NS/CC		175	320	103	20	
1% Ni-WP_2 NS/CC	Graphite rod	110	200	65	25	[19]
WP@NC NA	Graphite rod	110	156	50	90	This work

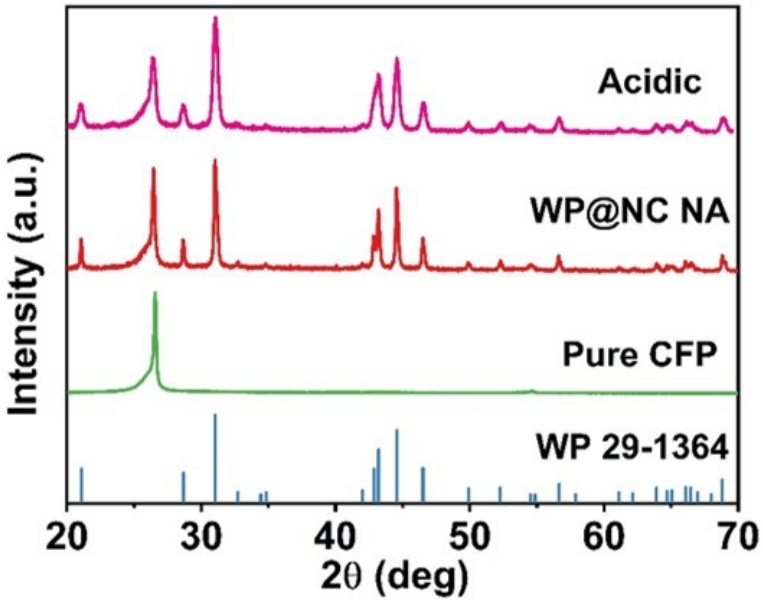

Figure S9. XRD pattern of WP@NC NA after the electrochemical measurement in 0.5 M H_2SO_4.

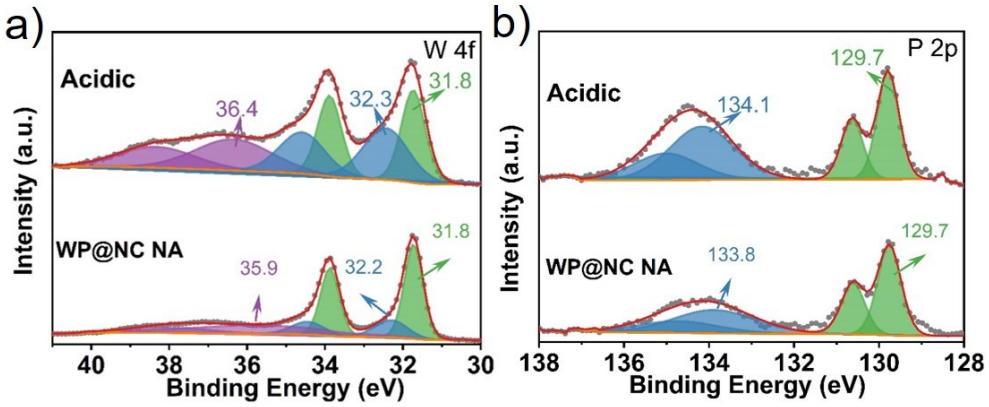

Figure S10. (a) W 4f window and (b) P 2p window XPS spectra of WP@NC NA after the electrochemical measurement in 0.5 M H_2SO_4.

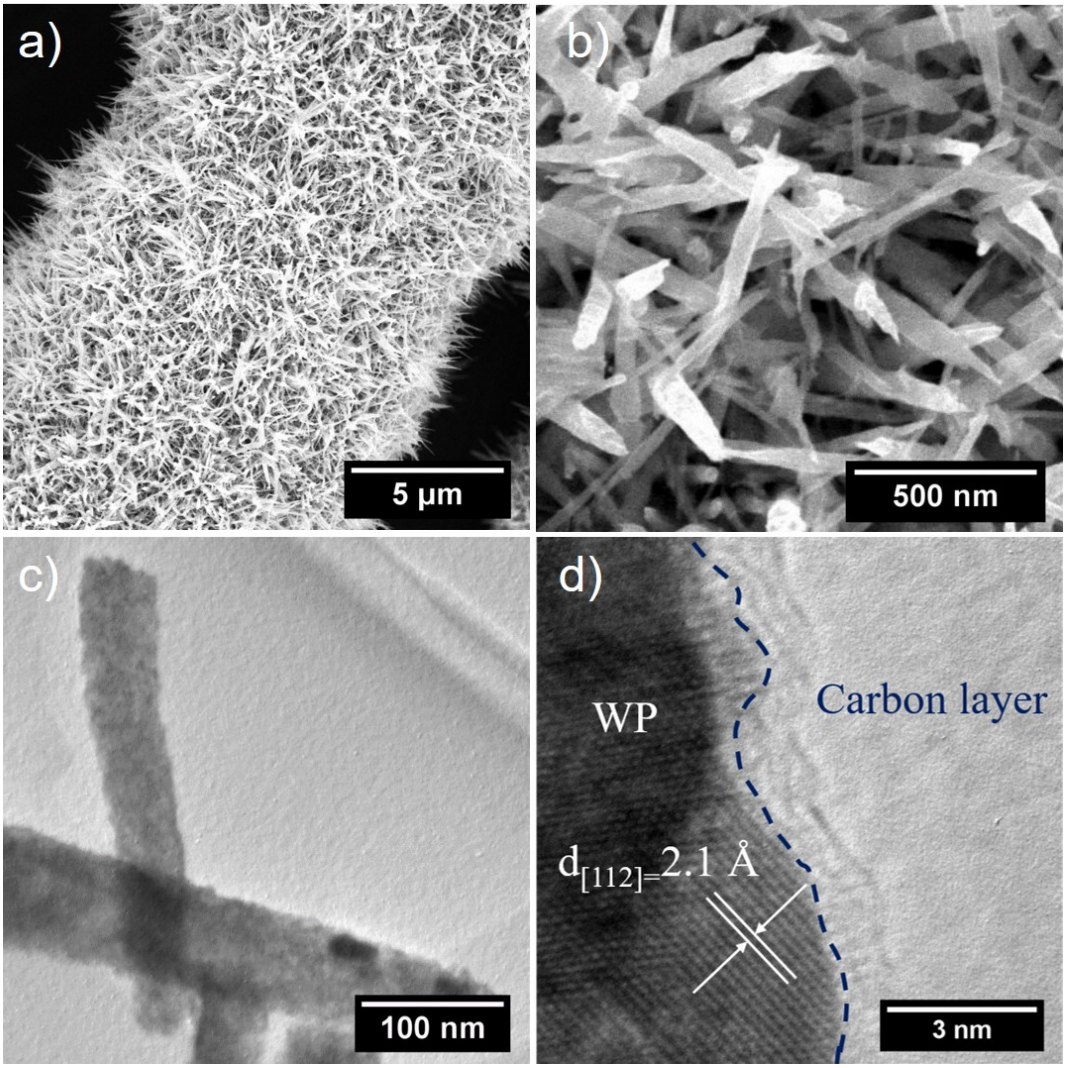

Figure S11. (a-b) SEM and (c-d) TEM images of WP@NC NA after long-term electrochemical measurement in 0.5 M H_2SO_4.

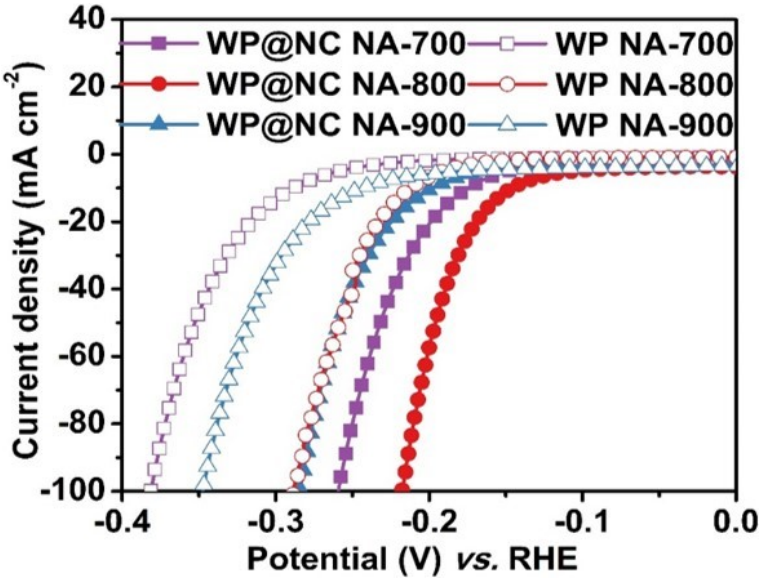

Figure S12. Polarization curves of WP@NC NA and WP NA obtained under different phosphidation temperatures (denoted as WP@NC NA-xx and WP NA-xx, where xx is the phosphidation temperature) in 1 M KOH. In the whole article, WP@NC NA-800 and WP NA-800 are also denoted as WP@NC NA and WP NA, respectively.

Table S2. Comparison of the HER activities of WP@NC NA with some representative highly efficient metal phosphides-based electrocatalysts in 1 M KOH electrolyte.

Catalyst	Counter electrode	η_{10} (mV)	η_{100} (mV)	Tafel slope (mV/dec)	Stability (h)	Reference
3D MoP/NPG	Pt wire	126	>300	56	12	[1]
MoP@NC	Graphite rod	106	>400	67	10	[2]
WP@NC		232	>400	88	--	
Co-WP	Graphite rod	119	>200	55	60	[3]
Mo-WP		175	>250	75	60	
N-MoP/CC	Graphite rod	70	~195	55	36	[6]
CoP@NPC/CP	Pt wire	152	~360	109	24	[7]
FeP@NPC/CP		~150	~480	--	10	
NiP@NPC/CP		~180	~400	--	10	
MoP/NC	Carbon rod	213	>250	61	12	[8]
WP_2 SMPs	Graphite rod	153	>250	60	5000 CVs	[9]
CFs@WP	Graphite rod	185	329	74	--	[15]
Ce-doped CoP	Graphite rod	92	~165	63.5	10	[12]
Ni_2P nanoarrays	Graphite rod	80	~140	24	76	[20]
$Co_{0.9}W_{1.1}P_2/C$	Graphite rod	54	--	59	50	[13]
$Co(OH)_x$@CoP	Graphite rod	100	~250	76	25	[21]
Fe-Ni_2P NSs	Carbon rod	116	200	74	12	[22]
HNP NiO/NiCoP	Pt foil	112	200	56	2000 CVs	[23]
H-CeO_{2-x}/Ni_2P @NC	Carbon rod	123	>250	60	27	[24]
exf-$MnPSe_3$	Pt	1000	>1100	--	100 CVs	[25]
Co-Co_2P@NPC /rGO	Carbon rod	~210	~440	--	19	[26]
CoP@NPCP	Platinum sheets	150	~380	20	25	[27]
WP@NC NA	Graphite rod	146	217	69	90	This work

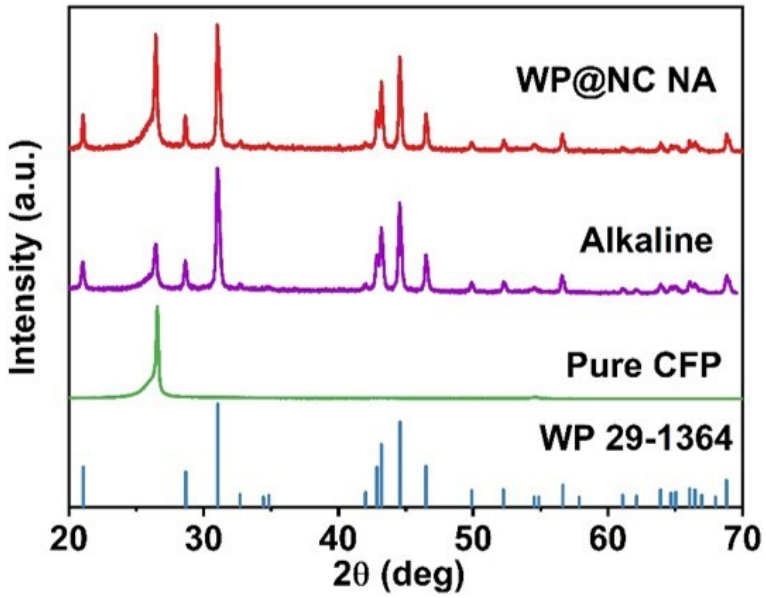

Figure S13. XRD pattern of WP@NC NA after the electrochemical measurement in 1 M KOH.

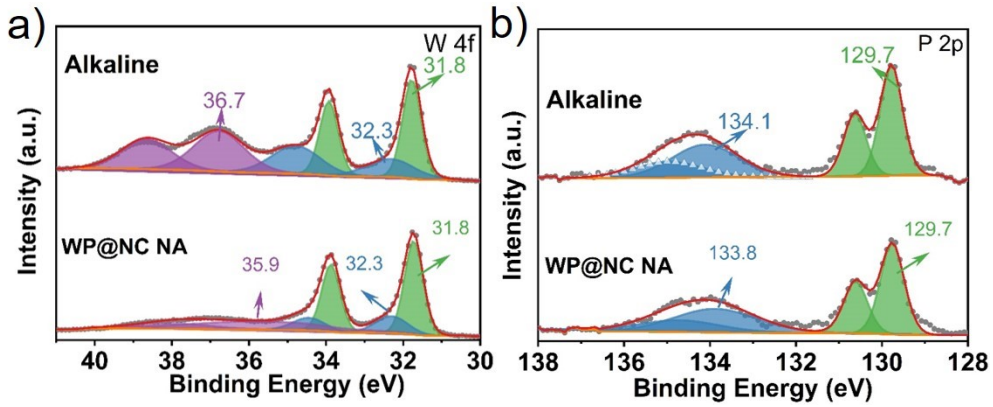

Figure S14. (a) W 4f window and (b) P 2p window XPS spectra of WP@NC NA after the electrochemical measurement in 1 M KOH.

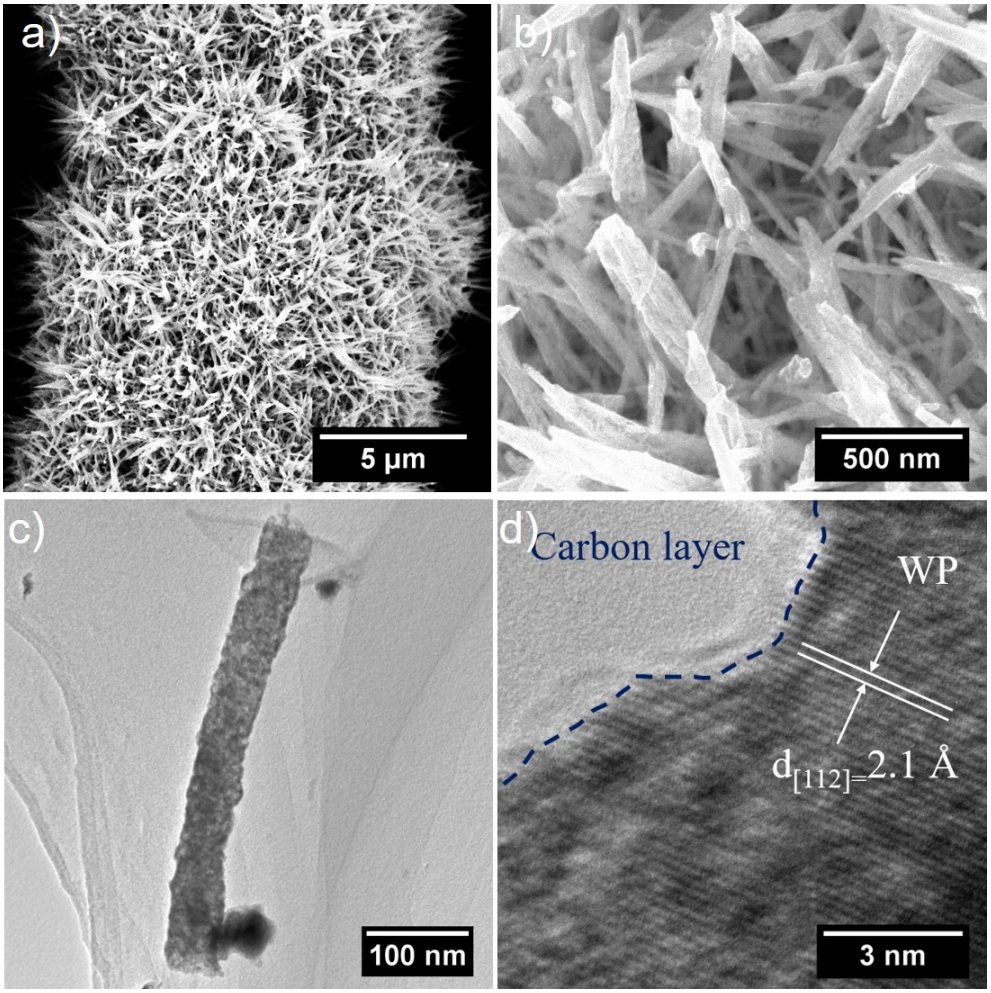

Figure S15. (a-b) SEM and (c-d) TEM images of WP@NC NA after long-term electrochemical measurement in 1 M KOH.

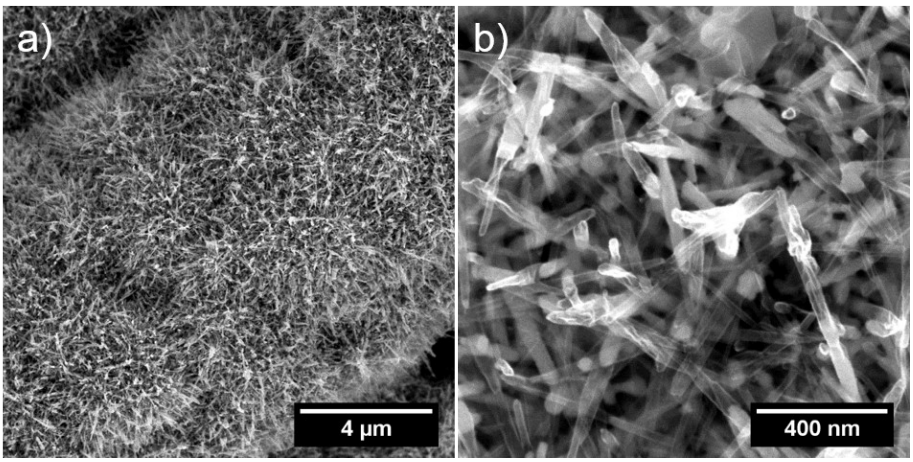

Figure S16. (a) Low- and (b) high-magnification SEM images of WP@C NA.

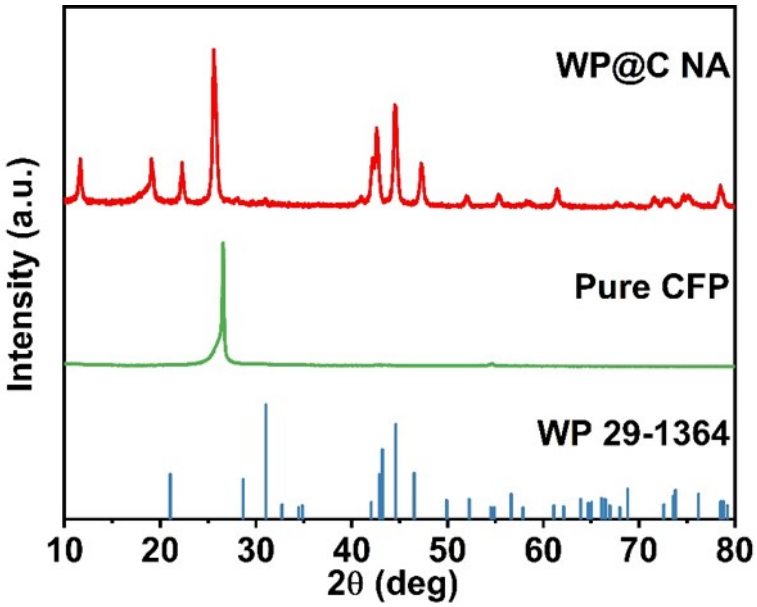

Figure S17. XRD pattern of WP@C NA.

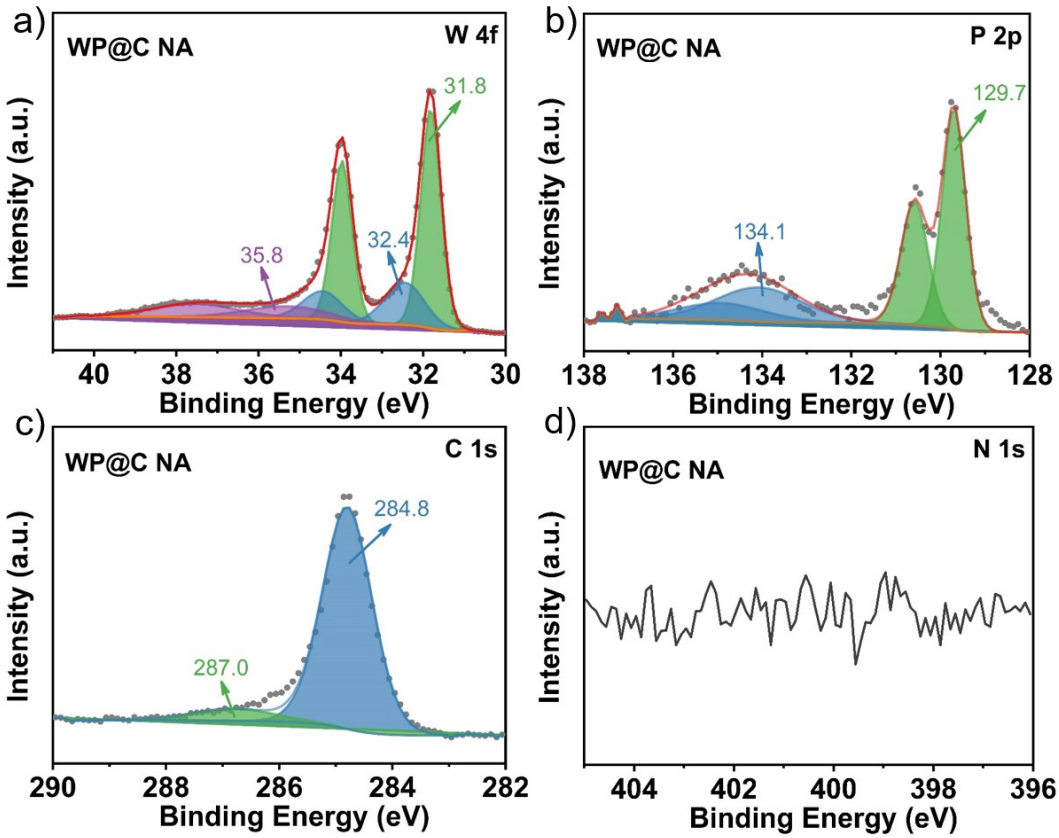

Figure S18. (a) W 4f window, (b) P 2p window, (c) C 1s window and (d) N 1s window of the XPS spectra of WP@C NA.

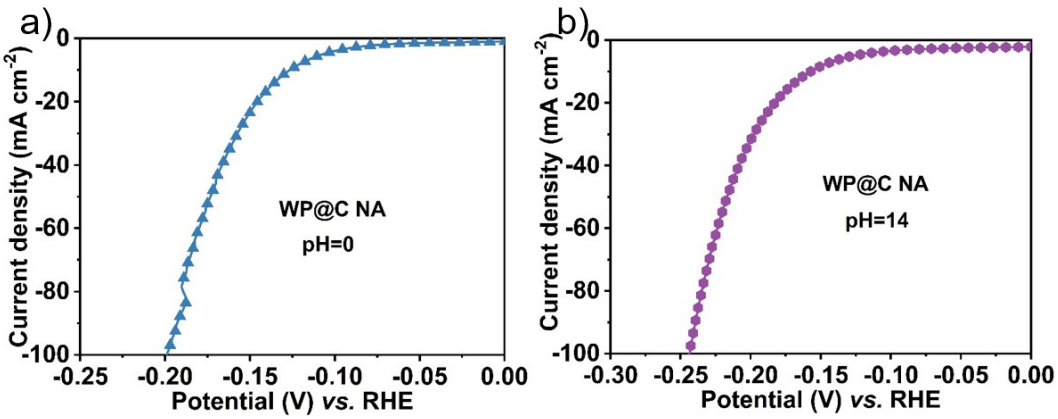

Figure S19. Polarization curves for the WP NA-s in (a) 0.5 M H_2SO_4 and (b) 1 M KOH.

All the potentials were corrected by iR drop.

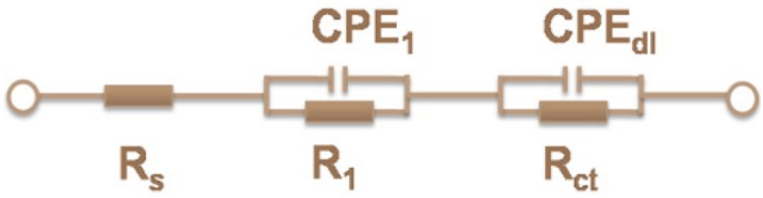

Figure S20. Equivalent circuit used to fit the EIS data. R_s is the overall series resistance, CPE_1 and R_1 are the constant phase element and resistance describing electron transport at GCE/electrocatalyst interface, respectively, CPE_{dl} is the constant phase element of the electrocatalyst/electrolyte interface, and R_{ct} is the charge transfer resistance at electrocatalyst/electrolyte interface.

Table S3. The fitting results of EIS spectra in 0.5 M H_2SO_4.

Sample	R_s (Ω)	Q_1 (F cm^{-2} S^{n-1})	n_1	R_1 (Ω)	Q_{ct} (F cm^{-2} S^{n-1})	n_{ct}	R_{ct} (Ω)
WP NA	0.79	3.878e-6	0.8902	2.60	0.08715	0.9183	15.74
WP@NC NA	0.01	1.58e-17	0.7868	2.86	0.01	0.9135	8.15

Supporting Discussion S2. Estimation of the electrochemical surface area (ECSA)

To measure the electrochemical capacitance, the potential was swept in the range 0.10 to 0.20 V *vs.* RHE at different scan rates. The capacitance current density ($\Delta J = J_a - J_c$ at 0.15 V *vs.* RHE) was plotted and the C_{dl} was obtained by a data fitting of the plot. ECSA was estimated from the C_{dl} using the specific capacitance value for a flat standard with 1 cm^2 of real surface area. In general, the C_{dl} for a flat surface ranges from 20 to 60 μF cm^{-2}, so in our calculations a specific capacitance for a flat surface area of 40 μF cm^{-2} was adopted.[28, 29]

$$ECSA = C_{dl}/40\ \mu F\ cm^{-2}$$

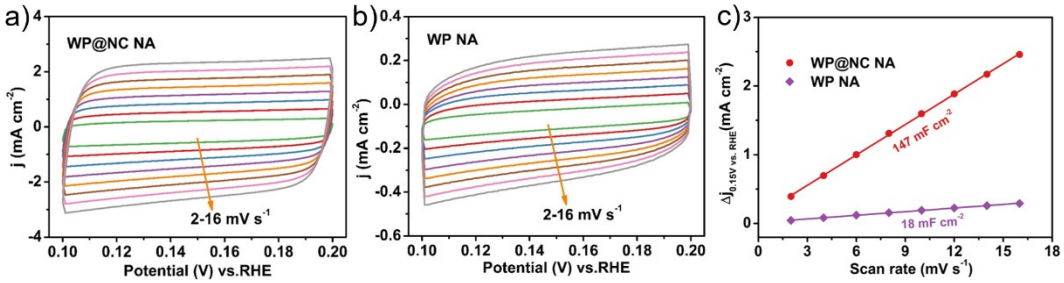

Figure S21. Cyclic voltammetry scans of (a) WP@NC NA and (b) WP NA in 0.5 M H_2SO_4. (c) Estimation of the C_{dl} through plotting the current density difference ($\Delta J = 1/2(J_a - J_c)$) at 0.15 V vs. RHE obtained from the CV against scan rate to fit a linear regression.

Table S4. The fitting results of EIS spectra in 1 M KOH.

Sample	R_s (Ω)	Q_1 ($F\ cm^{-2}\ S^{n-1}$)	n_1	R_1 (Ω)	Q_{ct} ($F\ cm^{-2}\ S^{n-1}$)	n_{ct}	R_{ct} (Ω)
WP NA	0.15	0.07541	0.6769	3.65	0.09023	0.9003	5.28
WP@NC NA	0.28	0.2751	0.6863	2.85	0.44	0.9713	3.50

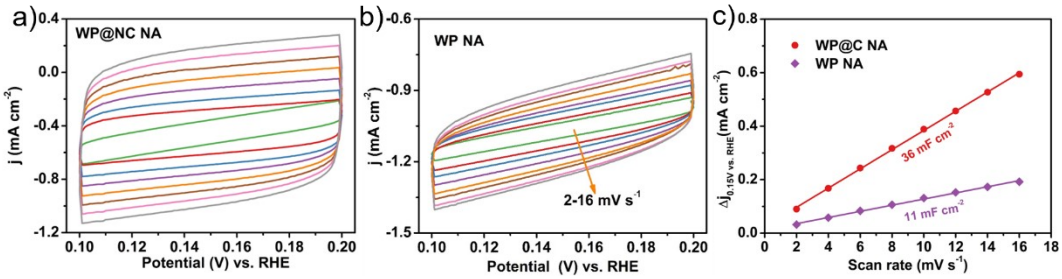

Figure S22. Cyclic voltammetry scans of (a) WP@NC NA and (b) WP NA in 1 M KOH. (c) Estimation of the C_{dl} through plotting the current density difference ($\Delta J = 1/2(J_a - J_c)$) at 0.15 V vs. RHE obtained from the CV against scan rate to fit a linear regression.

Supporting Discussion S3. Computational method and model

Density functional theory (DFT) calculations were conducted to optimize structures by Vienna ab initio simulation package (VASP).[30] The projector augmented wave (PAW) potentials with a planewave cutoff energy of 450 eV was implemented to compute the interaction between the ionic cores and valence electrons.[31, 32] The generalized gradient approximation (GGA) functional of Perdew–Burke–Ernzerhof (PBE) functional was applied as the exchange-correlation functional.[33] The grimme's semiempirical DFT-D3 dispersion correction was utilized to describe the van der Waals (vdW) interactions.[34] Based on the experiments, the (112) slab was chosen to model WP structure for HER reactions with the lattice parameters of a = 13.24 Å and b = 9.05 Å. To model the heterojunction of WP with nitrogen-doped graphene (CN), one layer of CN was construct on the top of WP (112). A vacuum layer of 15 Å was added to prevent the effects of two adjacent layers. The convergence criteria of electronic energies and atomic forces for all calculations were 10^{-5} eV and 0.03 eV $Å^{-1}$ and Gamma k-grid sampling of 3×3×1 was used for all geometry optimizations. To study the HER reaction pathways, in the acid condition, the *H is an important intermediate to evaluate the HER performance of the catalysts. While in alkaline condition, the *H_2O and *H+*OH and *H+OH^- intermediates will appear.

All of the intermediates were optimized by DFT calculation to obtain the energy of each structure. We use the computational hydrogen electrode (CHE) model proposed by Nørskov to calculate the Gibbs free energy of the intermediates.[35]

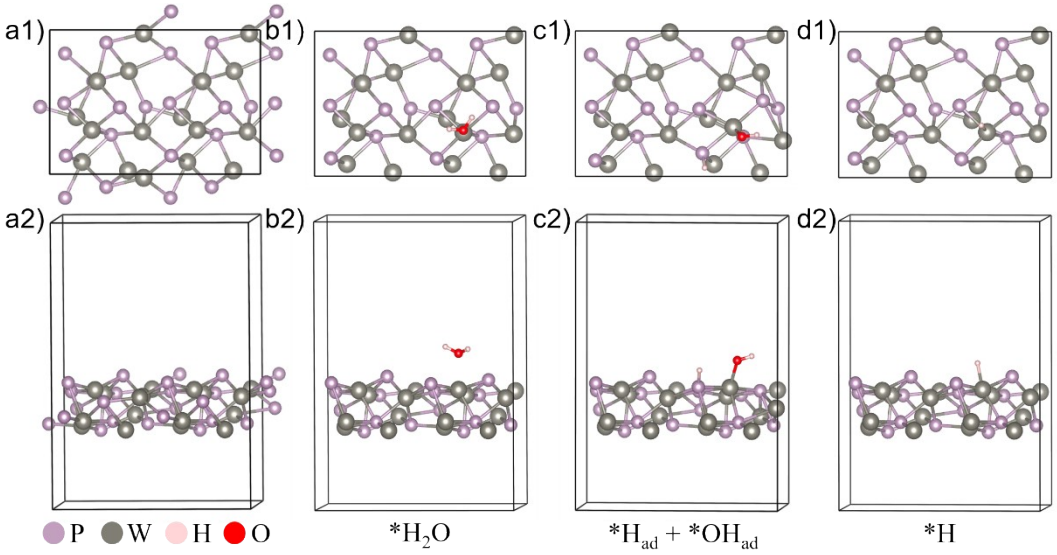

Figure S23. From left to right: top views and side views of (a) WP (112) surface model and (b) water adsorption, (c) water dissociation, (d) hydrogen adsorption on WP (112) surface.

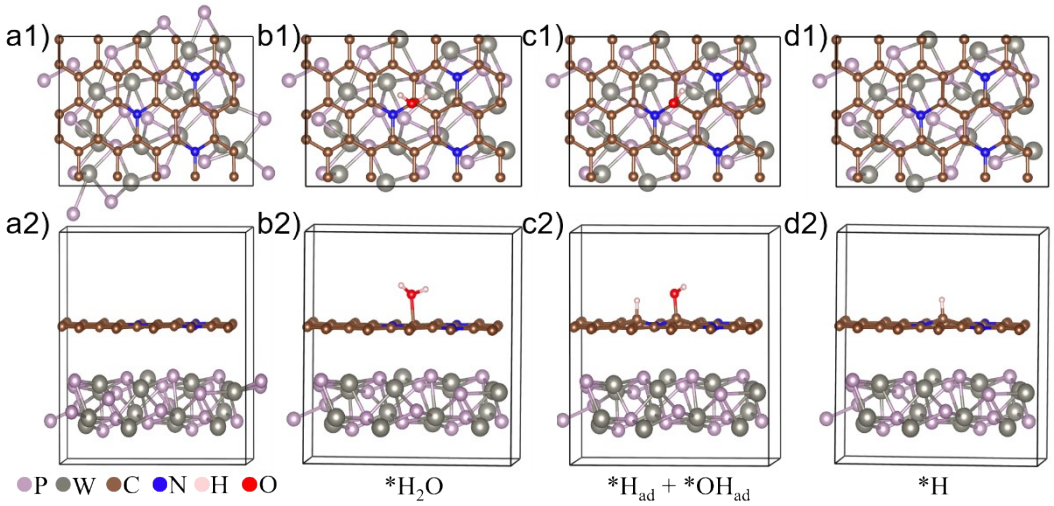

Figure S24. From left to right: top views and side views of (a) the model of WP (112) coated with one layer of nitrogen-doped graphene (NC) and (b) water adsorption, (c) water dissociation, (d) hydrogen adsorption on NC@WP (112) surface.

Reference

1. R. Ge, J. Huo, T. Liao, Y. Liu, M. Zhu, Y. Li, J. Zhang and W. Li, *Appl. Catal. B: Environ.*, 2020, **260**, 118196.
2. S. Chakrabartty, D. Sahu and C. R. Raj, *ACS Appl. Energy Mater.*, 2020, **3**, 2811-2820.
3. J. Wang, K. Chang, Z. Sun, J. H. Lee, B. M. Tackett, C. Zhang, J. G. Chen and C. Liu, *Appl. Catal. B: Environ.*, 2019, **251**, 162-167.
4. R. Wang, X. Y. Dong, J. Du, J. Y. Zhao and S. Q. Zang, *Adv. Mater.*, 2018, **30**, 1703711.
5. F. Sun, Y. Wang, L. Fang, X. Yang, W. Fu, D. Tian, Z. Huang, J. Li, H. Zhang and Y. Wang, *Appl. Catal. B: Environ.*, 2019, **256**, 117851.
6. N. Chen, W. Zhang, J. Zeng, L. He, D. Li and Q. Gao, *Appl. Catal. B: Environ.*, 2020, **268**, 118441.
7. J. Ren, G. Yuan, C. Weng and Z. Yuan, *Electrochim. Acta*, 2018, **261**, 454-463.
8. M. Lin, R. Lu, W. Luo, N. Xu, Y. Zhao and L. Mai, *ACS Appl. Energy Mater.*, 2021, **4**, 5486-5492.
9. Z. Xing, Q. Liu, A. M. Asiri and X. Sun, *ACS Catal.*, 2014, **5**, 145-149.
10. D. Huo, Z. Sun, Y. Liu, Z. Yu, Y. Wang and A. Wang, *ACS Sustain. Chem. Eng.*, 2021, **9**, 12311-12322.
11. Y. Liu, D. Zhang, K. Zhang, W. Dong, C. Tian and B. Mao, *J. Coord. Chem.*, 2020, **73**, 2590-2601.
12. W. Gao, M. Yan, H.-Y. Cheung, Z. Xia, X. Zhou, Y. Qin, C.-Y. Wong, J. C. Ho,

C.-R. Chang and Y. Qu, *Nano Energy*, 2017, **38**, 290-296.

13. B. Zhang, C. Li, J. Hu, D. Peng, K. Huang, J. Wu, Z. Chen and Y. Huang, *Nano Research*, 2021, **14**, 4073-4078.

14. S. S. Nkabinde, P. V. Mwonga, S. Mpelane, Z. B. Ndala, T. Kolokoto, N. P. Shumbula, O. Nchoe, R. R. Maphanga, K. I. Ozoemena, K. P. Mubiayi and N. Moloto, *New J. Chem.*, 2021, **45**, 15594-15606.

15. K. Xu, X. Fu, H. Li and Z. Peng, *Appl. Surf. Sci.*, 2018, **456**, 230-237.

16. M. Mohiuddin, A. Zavabeti, F. Haque, A. Mahmood, R. S. Datta, N. Syed, M. W. Khan, A. Jannat, K. Messalea, B. Y. Zhang, G. Chen, H. Zhang, J. Z. Ou and N. Mahmood, *J. Mater. Chem. A*, 2020, **8**, 2789-2797.

17. X. Zhang, T. Guo, T. Liu, K. Lv, Z. Wu and D. Wang, *Electrochim. Acta*, 2019, **323**, 134798.

18. W. Liu, P. Geng, S. Li, R. Zhu, W. Liu, H. Lu, S. Chandrasekaran, Y. Pang, D. Fan and Y. Liu, *Int. J. Hydrogen Energy*, 2020, **45**, 28576-28585.

19. W. Liu, P. Geng, S. Li, W. Liu, D. Fan, H. Lu, Z. Lu and Y. Liu, *J. Energy Chem.*, 2021, **55**, 17-24.

20. X. Yu, Z. Y. Yu, X. L. Zhang, Y. R. Zheng, Y. Duan, Q. Gao, R. Wu, B. Sun, M. R. Gao, G. Wang and S. H. Yu, *J. Am. Chem. Soc.*, 2019, **141**, 7537-7543.

21. L. Su, X. Cui, T. He, L. Zeng, H. Tian, Y. Song, K. Qi and B. Y. Xia, *Chem. Sci.*, 2019, **10**, 2019-2024.

22. X. Teng, L. Guo, L. Ji, J. Wang, Y. Niu, Z. Hu and Z. Chen, *ACS Appl. Energy Mater.*, 2019, **2**, 5465-5471.

23. M. Guo, Y. Qu, F. Zeng and C. Yuan, *Electrochim. Acta*, 2018, **292**, 88-97.

24. B. Zhang, H. Qin, L. Diao, N. Zhao, C. Shi, E. Liu and C. He, *J. Catal.*, 2019, **377**, 582-588.

25. R. Gusmão, Z. Sofer and M. Pumera, *Adv. Funct. Mater.*, 2019, **29**, 1805975.

26. G. Li, J. Yu, J. Jia, L. Yang, L. Zhao, W. Zhou and H. Liu, *Adv. Funct. Mater.*, 2018, **28**, 1801332.

27. L. Li, L. Song, H. Xue, C. Jiang, B. Gao, H. Gong, W. Xia, X. Fan, H. Guo, T. Wang and J. He, *Carbon*, 2019, **150**, 446-454.

28. C. Lv, Q. Yang, S. Xu, L. Yuan, Z. Huang, Z. Ren, J. Luo, S. Wang and C. Zhang, *Sustain. Energy Fuels*, 2021, **5**, 3373-3381.

29. Q. Dai, L. Wang, K. Wang, X. Sang, Z. Li, B. Yang, J. Chen, L. Lei, L. Dai and Y. Hou, *Adv. Funct. Mater.*, 2021, **DOI: 10.1002/adfm.202109556**.

30. G. Kresse and J. Furthmüller, *Matter Mater. Phys.*, 1996, **54**, 11169-11186.

31. P. E. Blöchl, *Phys. Rev. B*, 1994, **50**, 17953-17979.

32. D. Joubert, *Phys. Rev. B - Condens. Matter Mater. Phys.*, 1999, **59**, 1758-1775.

33. I. G. McKendry, R. Ding, S. L. Shumlas, J. P. Perdew, M. J. Zdilla, H. Peng, A. C. Thenuwara, D. R. Strongin and Q. Kang, *Proc. Natl. Acad. Sci.*, 2017, **114**, 9523-9528.

34. S. Grimme, J. Antony, S. Ehrlich and H. Krieg, *J. Chem. Phys.*, 2010, **132**, 154104.

35. J. K. Nørskov, J. Rossmeisl, A. Logadottir, L. Lindqvist, J. R. Kitchin, T. Bligaard and H. Jónsson, *J. Phys. Chem. B*, 2004, **108**, 17886-17892.